Journal of Solid State Chemistry 182 (2009) 153–159

Contents lists available at ScienceDirect

Journal of Solid State Chemistry

journal homepage: www.elsevier.com/locate/jssc

Crystal and magnetic structures of the brownmillerite compound $Ca_2Fe_{1.039(8)}Mn_{0.962(8)}O_5$

Farshid Ramezanipour [a,b], Bradley Cowie [a,b], Shahab Derakhshan [a,b], John E. Greedan [a,b,*], Lachlan M.D. Cranswick [c]

[a] Department of Chemistry, McMaster University, Hamilton, Ontario, Canada L8S 4M1
[b] Brockhouse Institute for Materials Research, McMaster University, Hamilton, Ontario, Canada L8S 4M1
[c] Canadian Neutron Beam Centre, National Research Council, Chalk River Laboratories, Chalk River, Ontario, Canada K0J 1J0

ARTICLE INFO

Article history:
Received 18 August 2008
Received in revised form
2 October 2008
Accepted 4 October 2008
Available online 22 October 2008

Keywords:
Ca_2FeMnO_5
Brownmillerite
Long range magnetic order
Crystal and magnetic structure
Neutron diffraction

ABSTRACT

The crystal and magnetic structures of the brownmillerite material, $Ca_2Fe_{1.039(8)}Mn_{0.962(8)}O_5$ were investigated using powder X-ray and neutron diffraction methods, the latter from 3.8 to 700 K. The compound crystallizes in *Pnma* space group with unit cell parameters of $a = 5.3055(5)$ Å, $b = 15.322(2)$ Å, $c = 5.4587(6)$ Å at 300 K. The neutron diffraction study revealed the occupancies of Fe^{3+} and Mn^{3+} ions in both octahedral and tetrahedral sites and showed some intersite mixing and a small, ~4%, Fe excess. While bulk magnetization data were inconclusive, variable temperature neutron diffraction measurements showed the magnetic transition temperature to be 407(2) K below which a long range antiferromagnetic ordering of spins occurs with ordering wave vector $k = (000)$. The spins of each ion are coupled antiferromagnetically with the nearest neighbors within the same layer and coupled antiparallel to the closest ions from the neighboring layer. This combination of intra- and inter-layer antiparallel arrangement of spins forms a G-type magnetic structure. The ordered moments on the octahedral and tetrahedral sites at 3.8 K are 3.64(16) and 4.23(16) μ_B, respectively.

1. Introduction

There has been considerable interest in materials with oxygen-deficient perovskite-related structures in recent years. Fuel cells and dense membranes for the partial oxidation of hydrocarbons are some of the areas of possible applications for these materials [1]. Brownmillerites are a family of oxygen-deficient compounds that form when a series of vacancies are introduced into the perovskite structure in an ordered manner. The result of the presence of these ordered arrays of vacancies is a structure involving alternating layers of octahedra and tetrahedra. The general formula for brownmillerites is $A_2MM'O_5$, where M and M' are octahedral and tetrahedral site cations, respectively, and A is a large cation residing in the spaces between the layers. The crystal structure involves both octahedral and tetrahedral layers alternating along the *b*-axis (Fig. 1). The octahedra share four equatorial corners with other octahedra within the layers. These layers are separated by chains of tetrahedra that run parallel to the *a*–*c* plane. The chains of tetrahedra are connected to the apical corners of octahedra from the layers above and below. Three space groups have been reported for brownmillerite materials, *Pnma*, *Ibm*2 and *Imma* and their variants [2–6]. The distinction arises due to the relative orientations of the tetrahedral chains as discussed by Greaves et al. [7] and Lambert et al. [8]. If the chains have the same orientation, one has the non-centric space group *Ibm*2, while if the chain orientations are opposite but ordered, *Pnma* is the choice and if the chains are disordered, *Imma* results. It has also been argued that materials which seem to be described in *Imma* actually contain ordered but modulated chains of the two orientations [8]. As well, the space group can change with composition and temperature. This has been documented for the brownmillerite series $Ca_2Fe_{2-x}Al_xO_5$ [9,10].

The magnetic properties of brownmillerites have been of interest, and detailed magnetic structure determinations for some brownmillerite systems have been performed. $Ca_2Fe_2O_5$ for example has been studied extensively during the past decades [11–13]. This material has a G-type antiferromagnetic structure, in which the spin on each atom is aligned antiparallel to all nearest neighbor spins (Fig. 2). This compound also shows a weak ferromagnetic component that has been attributed to the spin canting [11], where the angles between antiparallel spins are slightly different from 180°. The magnetic structure of Sr_2GaMnO_5 [14,15] has also been found to involve antiferromagnetic coupling

* Corresponding author at: Department of Chemistry, McMaster University, Hamilton, Ontario, Canada L8S 4M1. Fax: +1 905 521 2773.
E-mail address: greedan@mcmaster.ca (J.E. Greedan).

0022-4596/$ - see front matter © 2008 Elsevier Inc. All rights reserved.
doi:10.1016/j.jssc.2008.10.010

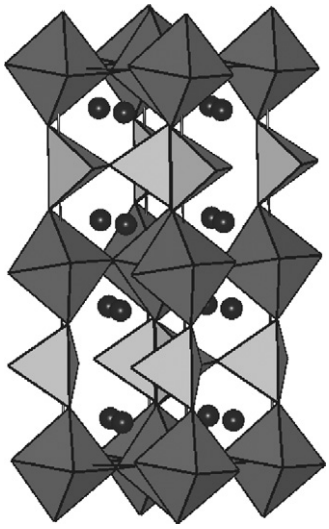

Fig. 1. Crystal structure of a brownmillerite. The corner-sharing octahedral layers (dark gray) are connected together through chains of corner-sharing tetrahedral (light gray). The counter ions are black spheres.

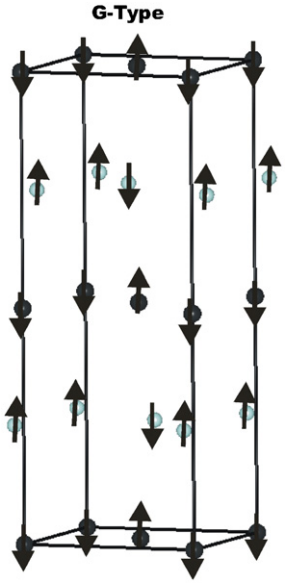

Fig. 2. The G-type magnetic structure of $Ca_2Fe_2O_5$. The octahedral and tetrahedral sites are shown by different colors. Each site couples antiferromagnetically with all nearest neighbors within the same layer and in the adjacent layers.

of Mn spins both within the planes and between the planes. This is an interesting case as the Mn^{3+} ions in two octahedral layers are separated by a non-magnetic Ga-containing tetrahedral layer. The distance between the Mn^{3+} ions on two neighboring layers is twice as long as the intra-layer distance. In addition, some small ferromagnetic domains within the antiferromagnetic system were suggested due to an anomaly in the magnetization versus temperature behavior [16]. A similar magnetic structure was found in the brownmillerite Ca_2MnAlO_5 [15]. A ferromagnetic component was also suggested for this system due to a divergence in the zero field and field cooled susceptibility data. This was considered as an indication of spin canting [15].

There is surprisingly little reported about the brownmillerite compound Ca_2FeMnO_5. Its crystal structure was studied using powder X-ray diffraction several years ago [17]. The unit cell constants are listed in Table 1 in square brackets. In a very recent work using Mössbauer spectroscopy a G-type magnetic structure has been proposed with the preferred spin direction along the *b*-axis [18]. The critical temperature was not reported. Also, unfortunately, the authors of [18] did not report the lattice constants of their sample and thus, the extent of oxidation is not known. In this paper the crystal and magnetic structures of this compound are studied using X-ray and neutron diffraction. Application of neutron diffraction provided information about the iron and manganese contents, and site occupancies of these ions in the crystal structure, to give the formula $Ca_2Fe_{1.039(8)}Mn_{0.962(8)}O_5$. As well, neutron diffraction provided a definitive determination of the magnetic structure, values for the ordered moments and also the critical temperature for magnetic ordering, as bulk magnetization data were ambiguous.

2. Experimental section

2.1. Synthesis

$Ca_2Fe_{1.039(8)}Mn_{0.962(8)}O_5$ was synthesized using $CaCO_3$ (99.99% Alfa Aesar), Fe_2O_3 (99.998% Alfa Aesar), and MnO (99.99% Alfa Aesar) as starting materials. The preparation was performed in two steps. Initially, the stoichiometric amounts of powders of the above reagents were weighed, ground together, pressed into a pellet and fired for 24 h at 1250 °C in air. The second step was performed by regrinding and heating the sample at 1250 °C under argon atmosphere for 48 h.

2.2. X-ray and neutron diffraction

A PANalytical X′Pert Pro MPD diffractometer with a linear X′Celerator detector was used for the X-ray powder diffraction study. The data were collected in a 2θ range of 5–90° with a 2θ step interval of 0.0084° using Cu$K\alpha_1$ radiation ($\lambda = 1.54056$ Å). Powder neutron diffraction measurements were performed on the C2 diffractometer at the Canadian Neutron Beam Centre at Chalk River, Ontario. The data were collected at 39 different temperatures starting from the base temperature, 3.8–700 K. A wavelength of 2.37150 Å, was used to obtain data within a 2θ range of 3.4–84.5° with a step size of 0.100°. The fine collimation data were also obtained at 300 and 550 K, using a wavelength of 1.33037 Å with a 2θ step interval of 0.050° in a 2θ range of 34.9–115°.

2.3. Magnetic property measurements

A quantum design MPMS SQUID magnetometer was used to obtain the magnetic data. The zero-field cooled and field cooled (ZFC/FC) magnetic susceptibility data were collected from 5 to 300 K on a powder sample in a gelatin capsule. The data were also collected from 300 to 700 K by heating and cooling in a furnace using a quartz sample holder, with an applied field of 1000 Oe. The isothermal magnetization data from 0 to 5.5 T were also obtained at three different temperatures.

Diamagnetic corrections of 8×10^{-6} emu/mol (Ca^{2+}), 10×10^{-6} emu/mol (Fe^{3+}), 10×10^{-6} emu/mol (Mn^{3+}) and 12×10^{-6} emu/mol (O^{2-}) were made to the susceptibility data [19].

3. Results and discussion

3.1. Crystal structure

The crystal structure of $Ca_2Fe_{1.039(8)}Mn_{0.962(8)}O_5$ was determined by powder X-ray and neutron diffraction. The Rietveld

refinement was performed using the GSAS program [20], employing the EXPGUI interface [21]. The space group *Pnma* has been previously reported for brownmillerites including Ca_2FeMnO_5 [17]. The presence of reflections such as (131) and (151), which violate I-centering indicate that this is the correct choice. Table 1 gives the final refinement results. The refinement was first performed on the powder X-ray diffraction data to obtain the cell parameters and metal positions to be used as input for refinement of the neutron data. Neutron diffraction has significant advantages here, as unlike for X-ray diffraction, there exists a strong contrast between Mn and Fe due to a very large difference between their scattering lengths: 9.45(2) fm for Fe and −3.75(2) fm for Mn. There were three very weak peaks in the neutron data indicating a very small amount of a side product that could not be identified due to its low concentration and possible peak overlaps. These peaks were excluded for the final refinement. Fig. 3 shows the observed, calculated and difference profiles for X-ray data, long wavelength neutron data ($\lambda = 2.37150$ Å) and fine collimation short wavelength neutron data ($\lambda = 1.33037$ Å) at 550 K, above the magnetic ordering temperature.

Table 1
The final refinement results for $Ca_2Fe_{1.039(8)}Mn_{0.962(8)}O_5$.

Space group	*Pnma*			
Z	4			
Lattice parameters	3.8 K	300 K	550 K	Ref. [17]
a (Å)	5.2985(4)	5.3055(5)	5.3251(1)	5.338
b (Å)	15.286(1)	15.322(1)	15.3865(3)	14.834
c (Å)	5.4530(5)	5.4587(5)	5.4787(1)	5.515
V (Å^3)	441.67(7)	443.74(7)	448.89(1)	436.69
R_{wp} (%)	5.95 ($\lambda = 2.37150$ Å)	4.62 ($\lambda = 1.33037$ Å) 2.28 (X-ray, $K\alpha_1$)	4.38 ($\lambda = 1.33037$ Å) 4.05 ($\lambda = 2.37150$ Å)	
Magnetic moments (μ_B)				
Mn	3.6(2)	2.7(1)		
Fe	4.2(2)	3.3(1)		
R_{mag} (%)	5.40	8.61		

Refinements at three different temperatures were performed on neutron data ($\lambda = 2.37150$ Å). Fine collimation data ($\lambda = 1.33037$ Å) were also obtained and refined at 550 and 300 K. In addition, a refinement of X-ray data was performed at 300 K using $K\alpha_1$ ($\lambda = 1.54056$ Å). The last column shows parameters from Nakahara et al. at ~300K [17].

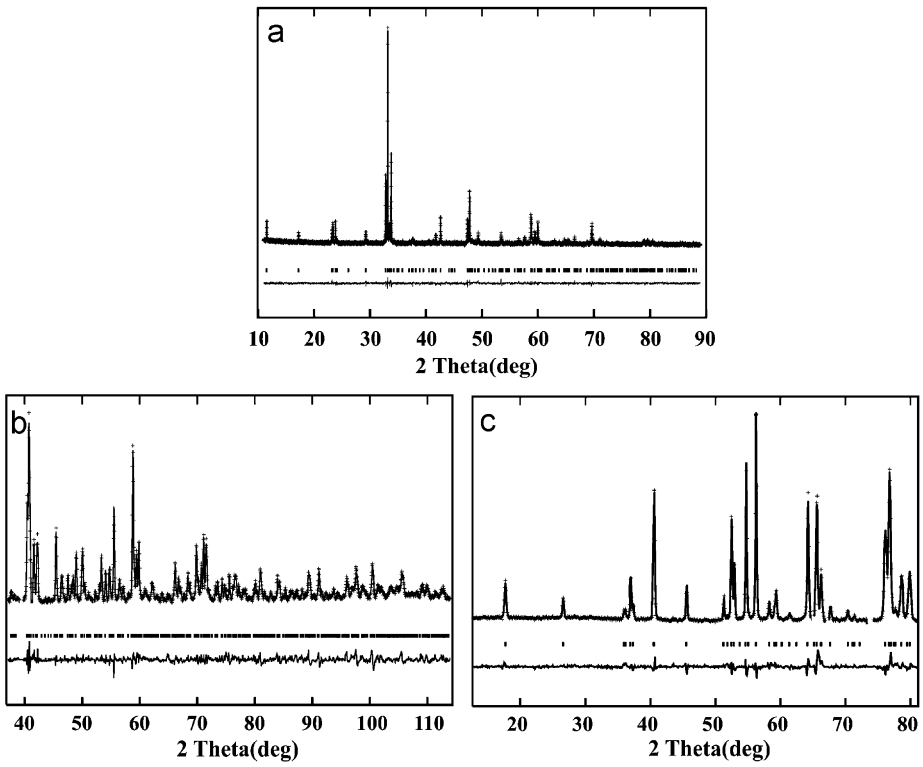

Fig. 3. Rietveld refinements of (a) powder X-ray diffraction data with $\lambda = 1.54056$ Å, (b) fine collimation neutron diffraction data with $\lambda = 1.33037$ Å (at 550 K), and (c) neutron data with $\lambda = 2.37150$ Å (at 550 K). The black dots are the experimental data, the solid line the model, the vertical tick marks locate Bragg peak positions and the lower line is the difference plot.

Initially, a fully ordered model with only Mn on the octahedral (O_h) site and Fe on the tetrahedral (T_d) site was refined as suggested in [17]. This resulted in a very large displacement factor, $U_{iso} = 0.150(8)\,Å^2$ at the O_h site, more than 10 times the value of any other site displacement factor, $R_{wp} = 0.0664$ and $\chi^2 = 2.50$. Two other models were tried: (1) Fe was added to the O_h site and (2) Fe and Mn were distributed over both sites. The results for (1) gave 14.8% excess Fe on the O_h site with $U_{iso} = 0.006(4)\,Å^2$, $R_{wp} = 0.0588$ and $\chi^2 = 2.21$. Model (2) gave for the contents of the O_h site, 86.8% Mn and 13.2% Fe, and for the T_d site, 90.6% Fe and 9.4% Mn with $U_{iso}(O_h) = 0.020(5)\,Å^2$, $U_{iso}(T_d) = 0.0115(11)$, $R_{wp} = 0.0557$ and $\chi^2 = 2.10$. Model (2) results in a slight excess of Fe, 4% overall. It is difficult to choose between (1) and (2) based only on the refinement results. Model (2) is closer to a 1:1 ratio for Fe and Mn as used in the synthetic mixture and there is no evidence for additional phases at the level of ~15% which would be demanded for Model (1). Thus, Table 2 gives a list of the atomic positions, site occupancies and the thermal displacement factors based on (2). Also a list of selected bond lengths and angles is given in Table 3.

In the octahedral layers the bonds parallel to the layers (equatorial bonds) are significantly shorter than those out of the planes (axial bonds). While it is tempting to attribute this to a static Jahn–Teller distortion, as the octahedral site mainly contains Mn^{3+}, in fact similar elongations are observed in most brownmillerites, even those for which the octahedral site contains only Fe^{3+}, a non-Jahn–Teller ion. In Table 4 the distortion indices (defined as the ratio of the axial bond length to the average equatorial bond length) are listed for Ca-based brownmillerites containing both Fe^{3+} and Mn^{3+} on the octahedral site. The index is significantly greater for the Mn^{3+} materials, indicating a role for a static Jahn–Teller component. The octahedra in $Ca_2Fe_{1.039(8)}Mn_{0.962(8)}O_5$ are distorted and octahedral angles show deviations of ~2° from the ideal angle of 90°. This is similar to the average deviation of bond angles in $Ca_2Fe_2O_5$, although the bond angles are distributed over a wider range in that compound [3].

In contrast to the octahedral layers, in the tetrahedral layers of $Ca_2Fe_{1.039(8)}Mn_{0.962(8)}O_5$ the bonds parallel to the layers (connected to the oxygens which are shared between two tetrahedra) are longer than the bonds out of the plane (connected to the oxygens shared between a tetrahedron and an octahedron). The tetrahedra are also distorted and deviations from the ideal angles of more than 4° are observed. The iron-only compound, $Ca_2Fe_2O_5$ shows a compression of the tetrahedra along the *b*-axis as well [3]. The distortion of the tetrahedra in that compound is less than that of $Ca_2Fe_{1.039(8)}Mn_{0.962(8)}O_5$.

The metal–oxygen bond distances obtained for $Ca_2Fe_{1.039(8)}Mn_{0.962(8)}O_5$ are consistent with tetrahedral Fe–O and octahedral Mn–O bond distances found in brownmillerites [3,15].

Bond valence calculations [25] give 3.164 for Mn and 2.885 for Fe which are in good agreement with the expected bond valence, 3, for both ions.

The unit cell parameters, especially the *b*-axis, for $Ca_2Fe_{1.039(8)}Mn_{0.962(8)}O_5$ differ markedly from those obtained previously [17], and the cell volume here is 1.4% larger. This indicates that the oxygen content of the sample in [17] is significantly greater than the sample here. Attempts to measure the oxygen content using reductive thermal gravimetry by heating the sample in a pure hydrogen gas stream at 900 °C resulted in a mixture of reduction products and the result was inconclusive. However, the study of $Ca_2GaMnO_{5+\delta}$ is relevant where a correlation was established between the unit cell volume and δ [26]. This calibration can be used to estimate δ in $Ca_2FeMnO_{5+\delta}$ for the sample in [17] which is ~0.2, a substantial level of oxidation.

Table 2
The atomic coordinates, site occupancies and displacement factors for $Ca_2Fe_{1.039(8)}Mn_{0.962(8)}O_5$ at 550 K

Atom	*x*	*y*	*z*	Occupancy	U_{iso} (Å^2)
Ca1	−0.012(1)	0.1101(2)	0.4802(8)	1.0	0.015(1)
Fe1	0.9484(7)	0.25	0.9353(6)	0.907(6)	0.012(1)
Mn1	0.0	0.0	0.0	0.868(5)	0.020(5)
Fe2	0.0	0.0	0.0	0.132(5)	0.020(5)
Mn2	0.9484(7)	0.25	0.9353(6)	0.094(6)	0.012(1)
O1	0.257(1)	−0.0125(2)	0.2388(6)	1.0	0.016(1)
O2	0.0210(7)	0.1424(2)	0.0653(6)	1.0	0.020(1)
O3	0.089(1)	0.25	0.6156(9)	1.0	0.024(2)

Table 3
Selected bond lengths (Å) and angles (°) for $Ca_2Fe_{1.039(8)}Mn_{0.962(8)}O_5$ at 550 and 300 K [...]

Mn1(Fe2)–O1	1.903(5) × 2 [1.901(6)]
Mn1(Fe2)–O1	1.939(5) × 2 [1.929(6)]
Mn1(Fe2)–O2	2.223(3) × 2 [2.206(5)]
Fe1(Mn2)–O2	1.844(3) × 2 [1.845(5)]
Fe1(Mn2)–O3	1.905(5) [1.905(8)]
Fe1(Mn2)–O3	1.935(5) [1.923(9)]
O1–Mn1(Fe2)–O1	92.15(2) × 2 [92.2(4)]
O1–Mn1(Fe2)–O1	87.85(2) × 2 [87.8(4)]
Mn1(Fe2)–O1–Mn1(Fe2)	167.8(2) [167.2(2)]
O2–Fe1(Mn2)–O2	127.8(3) [127.8(4)]
O2–Fe1(Mn2)–O3	105.8(2) × 2 [105.4(5)]
O2–Fe1(Mn2)–O3	105.3(2) × 2 [105.7(5)]
O3–Fe1(Mn2)–O3	104.8(2) [104.9(6)]
Fe1(Mn2)–O3–Fe1(Mn2)	121.4(3) [121.5(5)]

Table 4
Distortion indices for various Ca-based brownmillerites of Fe^{3+} and Mn^{3+}

Compound	Distortion index (see text)	Reference
Ca_2AlFeO_5	1.096	[5]
Ca_2GaFeO_5	1.084	[22]
$Ca_2Fe_2O_5$	1.084 (1.078)	[3,23]
Ca_2FeMnO_5	1.157	This work
Ca_2AlMnO_5	1.185	[24]
Ca_2GaMnO_5	1.172	[24]

3.2. Magnetic properties

The zero field cooled/field cooled (ZFC/FC) magnetic susceptibility data at a temperature range of 5–300 K are shown in Fig. 4a. The remarkable features in this diagram are a sudden increase in susceptibility at 125 K and the ZFC/FC divergence. The origin of these features is unclear. Susceptibility data were also collected in the range of 300–700 K (Fig. 4b). These data show a broad feature at 470 K, as well as a divergence between the data obtained from heating and cooling. However, these features can only correspond to short range ordering and no sharp transition was observed. Therefore, the magnetic transition temperature could not be found using the SQUID magnetometry data. Consequently, neutron diffraction was employed to study the magnetic properties as will be discussed later. A possible contamination of the sample by even small quantities of a magnetic side product can dominate the susceptibility data, and can also be partially responsible for some features such as ZFC/FC divergences.

The isothermal magnetization data were also collected at various temperatures (Fig. 5). A very weak hysteresis is present at 5, 50 and 310 K but the data at 500 K are linear and show no hysteresis, consistent with a typical paramagnetic system. Results for $Ca_2Fe_2O_5$ at 300 K, where spin canting is known to be present,

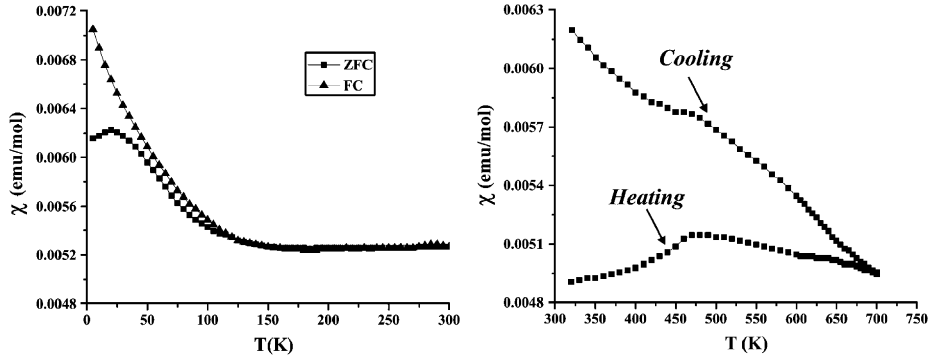

Fig. 4. (a) ZFC and FC molar susceptibility data within the temperature range of 5–300 K. Note the sudden upturn below 125 K. (b) The susceptibility data collected in furnace by heating and cooling in the field. The same feature is observed in both heating and cooling data at about 470 K.

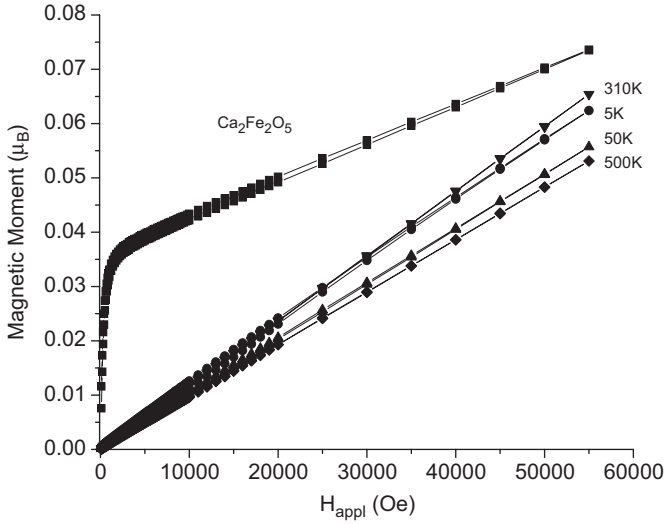

Fig. 5. Isothermal magnetization versus applied field behavior for Ca_2MnFeO_5 at various temperatures. Very weak hysteresis is observed at 5, 50 and 310 K. The 500 K data show a typical paramagnetic behavior. Results for $Ca_2Fe_2O_5$ at 300 K are shown for comparison.

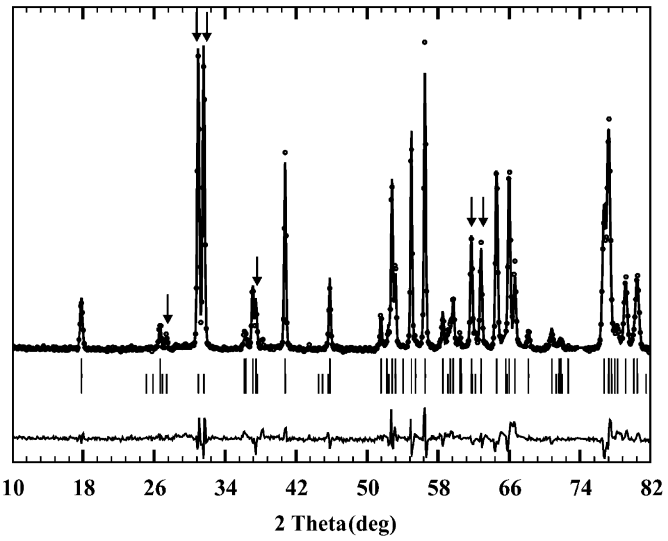

Fig. 6. The refinement result for the magnetic structure of $Ca_2Fe_{1.039(8)}Mn_{0.962(8)}O_5$ at 3.8 K. The most significant magnetic peaks are marked by arrows. The black dots are the experimental data; the solid line the model; two rows of the vertical tic marks locate Bragg peak positions for the crystal (top) and magnetic (bottom) structures and the lower line is the difference plot. The magnetic structure is confirmed as *G*-type (see Fig. 2) with the preferred moment direction along *b*. $R_{mag} = 0.054$ and the ordered moments on the octahedral and tetrahedral sites are 3.64(16) and 4.22(16) μ_B, respectively.

are included for comparison indicating that there is little evidence for significant sublattice canting in $Ca_2Fe_{1.039(8)}Mn_{0.962(8)}O_5$.

4. Neutron diffraction

Data were collected from 3.8 to 700 K, spanning the range of the susceptibility data. Fig. 6 shows data at 3.8 K where a number of magnetic reflections can be identified. The most significant of these (which are more intense than any structural reflections) appear at 30.99° and 31.60° and are indexed as (021)/(0−21) and (120)/(1−20), respectively. The other magnetic peaks are at 27.40° indexed as (110)/(1−10), 37.51° indexed as (−1−11)/(−111)/(1−11)/(111), 61.74° indexed as (−1−22)/(−122)/(1−22)/(122) and 62.83° indexed as (−2−21)/(−221)/(2−21)/(221). There is also a small peak at 38.2° that disappears at 149.5 K and is possibly related to the side product.

The magnetic structure of $Ca_2Fe_{1.039(8)}Mn_{0.962(8)}O_5$ was determined by refining the neutron diffraction data using the FullProf program [27], employing WinPLOTR [28]. A G-type magnetic structure model, Fig. 2, was verified. Fig. 6 shows the refinement results, $R_{mag} = 0.054$, for the magnetic structure. The spins on each site are oriented along the *b*-direction. The magnetic structure determined by neutron diffraction confirms that proposed from the Mössbauer study but of course provides much more detail [18].

By following the temperature dependence of the magnetic peak intensities, the critical temperature for long range order can be determined. The magnetic reflections disappear between 405 and 410 K. Plotting the refined magnetic moments of the *M* (mostly Mn^{3+}) and *M′* (mostly Fe^{3+}) sites as a function of temperature indicates $T_c = 407(2)$ K (Fig. 7). The ordered moments on the *M* and *M′* sites at 3.8 K are 3.64(16) and 4.22(16) μ_B, respectively, which agree reasonably with the spin only values, 2*S*, for $Mn^{3+}(S = 2)$ and $Fe^{3+}(S = 5/2)$, given some level of intersite mixing.

Above the transition temperature no long range ordering exists. However the presence of diffuse magnetic scattering at temperatures as high as 440 K (Fig. 8) is an indication of the presence of short range magnetic correlations which could explain in part the bulk susceptibility data which show no feature at T_c. Nonetheless, the bulk susceptibility is still difficult to understand

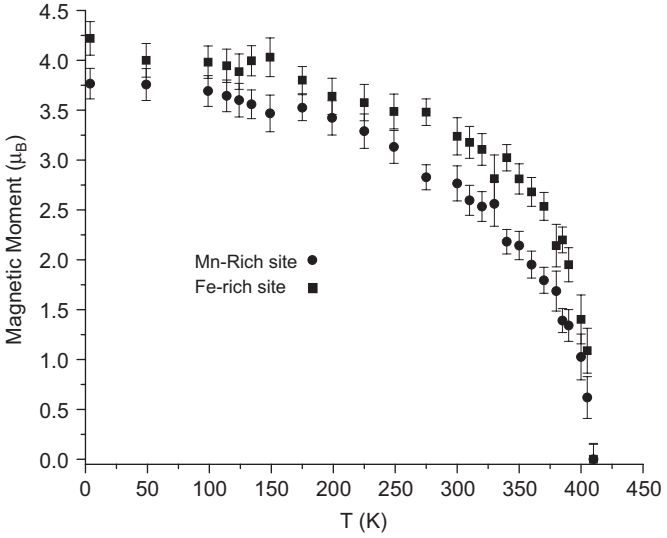

Fig. 7. Magnetic moments of Mn and Fe sites as functions of temperature. Note that the moments approach zero at about 407 K, indicating the magnetic transition temperature.

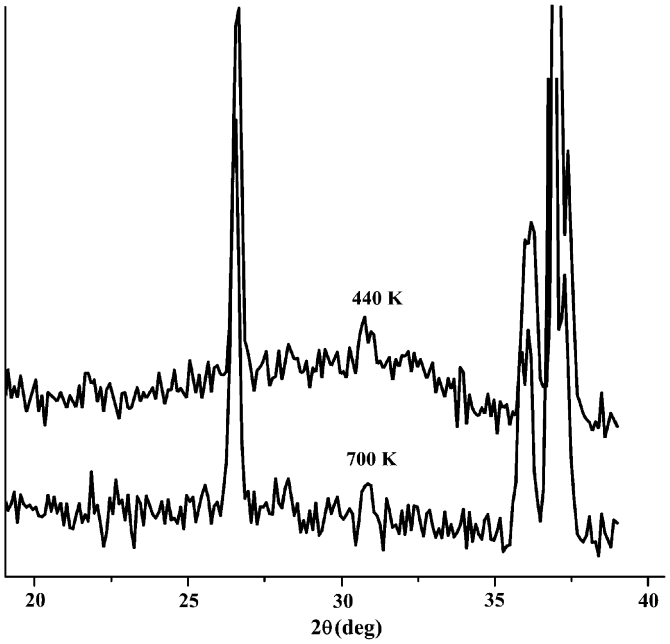

Fig. 8. Diffuse magnetic scattering at 440 K, compared to the data at 700 K. A noticeable hump appears at 440 K within 27–35 ° region, but is absent at 700 K.

and clearly provides little useful information regarding the true magnetic properties of this material. The presence of a small concentration of $Ca_2Fe_2O_5$ which would be difficult to detect due to peak overlap with Ca_2MnFeO_5 and which has $T_c = 725$ K and a weak ferromagnetic moment is a possible explanation of the bulk data.

The magnetic structure of $Ca_2Fe_{1.039(8)}Mn_{0.962(8)}O_5$ can be explained based on the principles of the superexchange mechanism. In this case the superexchange interactions will involve contributions from both t_{2g} and e_g orbitals [29]. Antiferromagnetic coupling of spins between two d^4, and two d^5 ions is expected as both σ and π superexchange pathways predict an antiparallel coupling of the two ions [30]. However the interaction between a d^4 and a d^5 ion in an ideal case (180°) can be ferromagnetic as the σ pathway of the superexchange will couple the two ions ferromagnetically [30]. However, crystal structural factors in $Ca_2Fe_{1.039(8)}Mn_{0.962(8)}O_5$ can diminish the ferromagnetic interactions. The distortion of superexchange pathways from linear is an important factor that needs to be taken into account. The M–O–M and M'–O–M' angles show large deviations from 180° (Table 3). It should be noted that even though some mixing of ions exists, the majority of octahedral sites are still occupied by Mn and the majority of tetrahedral sites are occupied by Fe, and therefore the Mn–Fe interactions are mostly inter-layer interactions. The inter-layer superexchange angle M–O–M' is 144.35°, a significant distortion from linearity. These distortions are direct results of the layered structure of brownmillerites. Unlike the perovskite structure that involves corner sharing of only octahedra, the brownmillerite structure needs to accommodate the corner sharing of both octahedra and tetrahedra and that imposes a large amount of twisting to the bond angles. The geometric features of tetrahedra do not allow the formation of linear bond angles while corner sharing with other tetrahedra and octahedra exists.

5. Summary and conclusions

The crystal and magnetic structures of the brownmillerite compound $Ca_2Fe_{1.039(8)}Mn_{0.962(8)}O_5$ were determined. Neutron diffraction showed small levels of mixing of Mn and Fe in both octahedral and tetrahedral sites and an overall ~4% Fe excess. The compound shows a long range antiferromagnetic ordering below the transition temperature, 407(2) K. The magnetic structure of this compound involves both intra- and inter-layer antiferromagnetic coupling of nearest neighbor spins forming a G-type magnetic structure. The ordered moments at 3.8 K are 3.64(16) and 4.22(16) μ_B for the octahedral and tetrahedral sites, respectively. The possible intra-layer Fe^{3+}–Mn^{3+} ferromagnetic coupling predicted by the superexchange mechanism is not evident due perhaps to the large deviations from linearity of superexchange pathways as a result of the structural constraints of a brownmillerite system.

Acknowledgments

We thank the Natural Sciences and Engineering Research Council of Canada for a Discovery Grant to J.E.G. and Major Resource Access Grants to the Canadian Neutron Beam Centre and the Brockhouse Institute for Materials Research.

References

[1] J. Malveiro, T. Ramos, L.P. Ferreira, J.C. Waerenborgh, M.R. Nunes, M. Godinho, M.D. Carvalho, J. Solid State Chem. 180 (2007) 1863–1874.
[2] E.F. Bertaut, P. Blum, A. Sagnieres, Acta Crystallogr. 12 (1959) 149–159 (PNMA).
[3] J. Berggren, Acta Chem. Scand. 25 (1971) 3616–3624.
[4] D.K. Smith, Acta Crystallogr. 15 (1962) 1146–1152 (IMMA).
[5] A.A. Colville, S. Geller, Acta Crystallogr. B 27 (1971) 2311–2315 (IBM2).
[6] F. Lindberg, S.Y. Istomin, P. Berastegui, G. Svensson, S.M. Kazakov, E.V. Antipov, J. Solid State Chem. 173 (2003) 395–406.
[7] C. Greaves, A.J. Jacobson, B.C. Tofield, B.E.F. Fender, Acta Crystallogr. B 31 (1975) 641–646.
[8] S. Lambert, H. Leligny, D. Grebille, D. Pelloquin, B. Raveau, Chem. Mater. 14 (2002) 1818–1826.
[9] K. Fukuda, H. Ando, J. Am. Ceram. Soc. 85 (2002) 1300–1302.
[10] G.J. Redhammer, G. Tippelt, G. Roth, G. Amthauer, Am. Mineral. 89 (2004) 405–420.
[11] T. Hirone, J. Appl. Phys. 36 (1965) 988–992.
[12] T. Takeda, Y. Yamaguchi, S. Tomiyoshi, M. Fukase, M. Sugimoto, H. Watanabe, J. Phys. Soc. Jpn. 24 (1968) 446–452.

[13] P. Berasteguil, S.G. Eriksson, S. Hull, Mater. Res. Bull. 34 (1999) 303–314.
[14] D.V. Sheptyakov, A.M. Abakumov, E.V. Antipov, A.M. Balagurov, S.J.L. Billinge, P. Fischer, L. Keller, M.V. Lobanov, B.Ph. Pavlyuk, V.Yu. Pomjakushin, M.G. Rozova, Appl. Phys. A 74 (2002) S1734–S1736.
[15] A.J. Wright, H.M. Palmer, P.A. Anderson, C. Greaves, J. Mater. Chem. 12 (2002) 978–982.
[16] A.J. Wright, H.M. Palmer, P.A. Anderson, C. Greaves, J. Mater. Chem. 11 (2001) 1324–1326.
[17] Y. Nakahara, S. Kato, M. Sugai, Y. Ohshima, K. Makino, Mater. Lett. 30 (1997) 163–167.
[18] A.I. Rykov, K. Nomura, Y. Ueda, A.N. Vasiliev, J. Magn. Magn. Mater. 320 (2008) 950–956.
[19] P.W. Selwood, Magnetochemistry, second ed., Interscience Publishers, Inc., New York, 1996.
[20] A.C. Larson, R.B. Von Dreele, General Structure Analysis System (GSAS), Los Alamos National Laboratory Report LAUR, 1994, pp. 86–748.
[21] B.H. Toby, J. Appl. Crystallogr. 34 (2001) 210–213.
[22] R. Arpe, Hk. Müller-Buschbaum, R.V. Schenck, Z. Anorg. Allg. Chem. 410 (1974) 97–103.
[23] P. Berastegui, S.-G. Eriksson, S. Hull, Mater. Res. Bull. 34 (1999) 303–314.
[24] A.M. Abakumov, M.G. Rozova, E.V. Antipov, Russ. Chem. Rev. 73 (2004) 847–860.
[25] I.D. Brown, D. Altermatt, Acta Crystallogr. B 41 (1985) 244–247.
[26] A.M. Abakumov, M.G. Rozova, B.Ph. Pavlyuk, M.V. Lobanov, E.V. Antipov, O.I. Lebedev, G. van Tendeloo, D.V. Sheptyakov, A.M. Balagurov, F. Bouree, J. Solid State Chem. 158 (2001) 100.
[27] T. Roisnel, J. Rodriguez-Carvajal, FULLPROF ver 1.9c: Rietveld, Profile Matching & Integrated Intensity Refinement of X-ray and/or Neutron Data, Laboratoire Léon Brillouin, Saclay, France, 2001.
[28] T. Roisnel, J. Rodríguez-Carvajal, WinPLOTR: a Windows tool for powder diffraction patterns analysis, in: R. Delhez, E.J. Mittenmeijer (Eds.), Proceedings of the Seventh European Powder Diffraction Conference (EPDIC 7), Materials Science Forum, 2000, pp. 118–123.
[29] R.L. Martin, in: H.J. Emeleus (Ed.), New Pathways in Inorganic Chemistry, Cambridge University Press, Cambridge, 1968.
[30] J.B. Goodenough, Magnetism and the Chemical Bond, Interscience, New York, 1963.